Hydrogen production for fuel cells by autothermal reforming of methane over sulfide nickel catalyst on a gamma alumina support

D.L. Hoang *, S.H. Chan, O.L. Ding

Fuel Cell Strategic Research Programme, School of Mechanical & Aerospace Engineering, Nanyang Technological University, 50 Nanyang Avenue, 639798 Singapore, Singapore

Abstract

Experimental and modelling studies have been conducted on catalytic autothermal reforming (ATR) of methane for hydrogen production over a sulfide nickel catalyst on a gamma alumina support. The experiments are performed with different feedstock under thermally neutral conditions. The results show that the performance of the reformer is dependent on the molar air-to-fuel ratio (A/F), the molar water-to-fuel ratio (W/F) and the flowrate of the feedstock mixture. The optimum conditions for high methane conversion and high hydrogen yield are A/F = 3–3.5, W/F = 2–2.5 and a fuel flowrate below 120–250 l h^{-1}. Under these conditions, a methane conversion of 95–99% and a hydrogen yield of 39–41% on a dry basis can be achieved and 1 mole of methane can produce 1.8 moles of hydrogen at an equilibrium reactor temperature of not exceeding 850 °C.

A two-dimensional reactor model is developed to simulate the conversion behaviour of the reactor for further study of the reforming process. The model includes all aspects of the major chemical kinetics and the heat and mass transfer phenomena in the reactor. The predicted results are successfully validated with experimental data.
© 2005 Elsevier B.V. All rights reserved.

Keywords: Methane; Autothermal reforming; Two-dimensional catalytic modelling; Hydrogen production; Fuel cell reactor

1. Introduction

Fuel cell technology has been of special interest in recent years due to its higher efficiency in energy conversion and no/less harmful emissions compared with other energy conversion systems. All fuel cells are either fed by pure hydrogen from a storage vessel or by hydrogen-rich gas produced from widely available fuels via a reforming process. A direct supply of pure hydrogen is desirable for fuel cell. Nevertheless, hydrogen storage still remains a challenge as the fuel has a very low energy density under normal ambient conditions, and this makes storage difficult for mobile applications. Therefore, a reliable method to ensure a steady supply of hydrogen for mobile fuel cells is to use reforming techniques, which extract hydrogen from hydrocarbon fuels such as methane.

Three major thermo-chemical reforming techniques are used to produce hydrogen from methane and other hydrocarbon fuels

[1,2], i.e., steam reforming (SR), partial oxidation (PO) and autothermal reforming (ATR). The steam reforming of methane has been studied extensively [3–6]. It is probably the most common and traditional method for producing hydrogen on an industrial scale. Though this process can yield high a concentration of hydrogen (up to 70% on a dry basis), it is strongly endothermic and, hence, requires a substantial supply of external heat. Therefore, a reforming system with a heat-exchanger becomes very bulky and heavy, and it has high thermal inertia for frequent start-up and shutdown operation. As a result, it is not so suitable for a mobile fuel cells. Partial oxidation [7–10] does not have the disadvantage of being endothermic, but it produces a high carbon monoxide concentration [7] that is undesirable for polymer electrolyte membrane fuel cells.

Autothermal reforming [11–16] combines the thermal effects of the PO and SR reactions by feeding the fuel, water and air together into the reactor. The thermal energy generated from PO is absorbed by SR and hence the overall temperature is lower. This is favourable for the water-gas shift reaction which consumes carbon monoxide and produces more hydrogen [7,11].

---

* Corresponding author.
  E-mail address: pt404215@ntu.edu.sg (D.L. Hoang).

Nomenclature

b	thickness of the reactor wall (m)
C_i	mole fraction of gas (i)
c_{pg}	heat capacity of gas (J kg^{-1} K^{-1})
c_{pb}	heat capacity of catalyst bed (J kg^{-1} K^{-1})
D_i	gas diffusivity of species i (m^2 s^{-1})
D_{dpi}	dispersion coefficient (m^2 s^{-1})
d_p	catalyst pellet diameter (m)
E_j	activation energy of reaction j (kJ kmol^{-1})
ΔH_i	adsorption enthalpy of species i (kJ kmol^{-1})
ΔH_j	heat of reaction j (kJ kmol^{-1})
h	heat transfer coefficient (W m^{-2} K^{-1})
h_i, h_o	heat transfer coefficient on the inside and outside of reactor wall (W m^{-2} K^{-1})
K	heat conduction coefficient of catalyst bed (W m^{-1} K^{-1})
K_{ej}	equilibrium constant of reaction j (j = 2, 3, 4)
K_{CH_4}	adsorption constant
K_{oi}, K_{oj}	constant
$K_{CH_4}^C$	adsorption constant
k_g	heat conduction coefficient of gas (W m^{-1} K^{-1})
k_j	rate constant of reaction j
k_{oj}	constant
p_{CH_4}	partial pressure CH$_4$ (bar)
R	universal gas constant (kJ kmol^{-1} K^{-1})
R_j	rate of reaction j (kmol kgcat^{-1} h^{-1})
r	radial coordinate (m)
r_i	conversion rates of species i (kmol kgcat^{-1} h^{-1})
S_h	heat transfer area per volume of catalyst bed (m^2 m^{-3})
T, T_g	temperatures of catalyst and bulk gas (K)
T_a	surrounding temperature (K)
T_a	outer reactor wall and surrounding temperatures (K)
u	superficial gas velocity (m s^{-1})

Greek symbols

α	overall heat transfer coefficient through the reactor wall (W m^{-2} K^{-1})
ε	void fraction of catalyst bed
λ	heat conduction coefficient through the wall
ρ_{cat}	catalyst density (kg m^{-3})
ρ_b	catalyst bed density (kg m^{-3})
ρ_g	gas density (kg m^{-3})

Subscripts

a	ambient air
cat	catalyst
g	gas
i	gas species
j	reaction index (1–4)
r, z	axes cylindrical coordinate
s	solid phase

Hence, the autothermal reactor is more compact and practical for use with mobile fuel cells.

The objective of this study is to investigate the performance of ATR of methane over a sulfide nickel catalyst on a gamma alumina support under thermally neutral conditions with different compositions of feedstock. Modelling work is also carried out to study further the conversion behaviour inside the reactor.

2. Experimental study

2.1. Equipment

The schematic layout of the equipment used in this study is shown in Fig. 1. The flowrates of air, methane and water are automatically controlled by a computer according to set values. The fed mixture is heated by either an electrical heater in the start-up stage or by hot reformate gas under steady operations to ensure that water is in vapour phase when entering the reactor.

The reactor is essentially a stainless-steel tube (inner diameter = 30 mm, length = 200 mm) that is filled with a sulfide nickel catalyst. Reactor temperature is measured at 5 points along its centre length by five thermocouples. The outer reactor wall and all the gas pipes are covered by thermal insulation to minimize heat losses. The reactor operates under atmospheric pressure. The reformate sample gas is channelled to a system of analyzers, at which its compositions is measured.

2.2. Catalyst

The catalyst was a commercial sulfide nickel catalyst Ni-0309S, supported on gamma alumina and was supplied by Engelhard. This is a new type of commercial catalyst that is specially used for hydrogen production from hydrocarbon fuel reforming. The reasons for choosing this catalyst is that it is highly active and relatively cheap and has prospective use in industries compared with other types of conventional nickel/alpha alumina catalyst. The catalyst is of spherical shape and is ready for use as supplied. The amount of catalyst loaded in the reactor was 68 g. The physical properties of the catalyst are listed in Tables 1a and b.

2.3. Experimental procedure

To operate the reactor, only methane at a flowrate of 2 l min^{-1} and air with an air-to-fuel ratio (A/F) of 6 are supplied initially to the reactor where the mixture is ignited by sparks from a spark-plug. Heat released from methane combustion heats up the catalyst bed. When the average catalyst temperature reaches about 700 °C, steam is added to the inlet mixture and then methane, and the A/F and molar water-to-fuel (W/F) ratios are adjusted to the desired values for testing. The feedstock conditions are varied in the range that ensures that the reactor sustains a thermally neutral operation between 500 °C and 900 °C. Based on a theoretical analysis of the optimum conditions for autothermal reforming of methane [11], the A/F is varied from 2.5 to 5 and the W/F is varied at each A/F. The W/F is increased step-by-step with increments of 0.5 from a starting value of 1 with
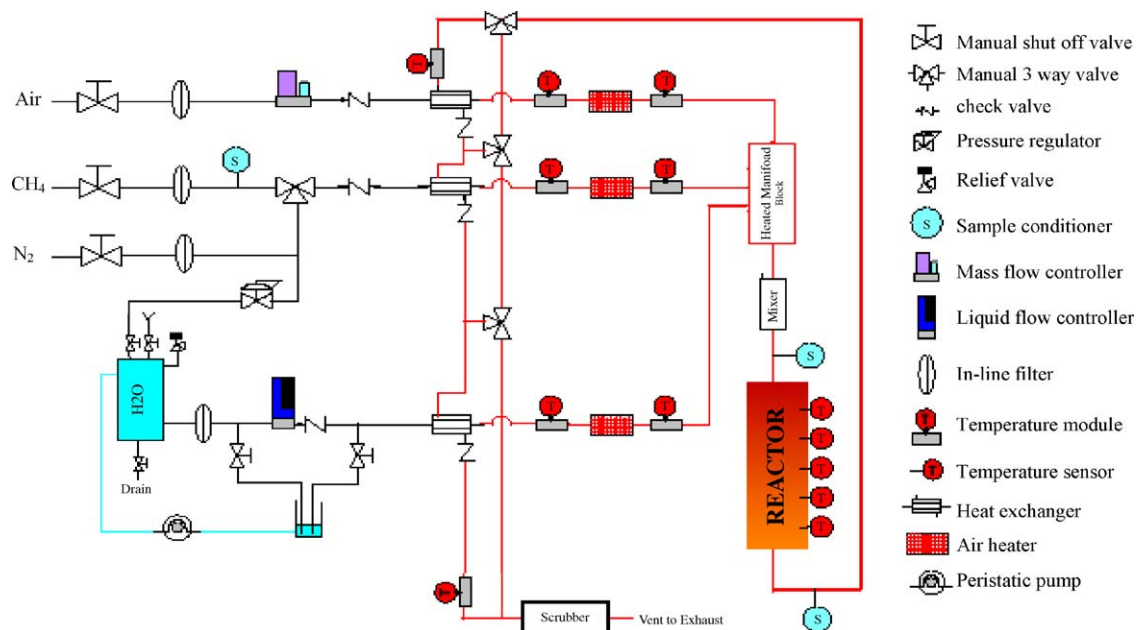
Fig. 1. Schematic layout of the rig.

Table 1a
Catalyst properties

Nickel content (wt.%)	9.8
Sulfur content (wt.%)	4.9
Alumina content (wt.%)	Balance
Surface area ($m^2 g^{-1}$)	155
Total pore volume ($m g^{-1}$)	0.9
Size of the sphere (mm)	1.75
Average crush strength (N)	25

a time interval between successive steps of at least 30 min for the reactor to reach a steady-state condition. The reformate gas concentration is recorded. The W/F is increased until the reactor cannot sustain autothermal reactions.

2.4. Experimental results

The extensive experimental data were recorded and processed. Typical results under a methane flowrate of $120 l h^{-1}$ are expressed in Figs. 2–15. These show the effect of the A/F the W/F on the performance of the autothermal reactor.

The variation of wet and dry product gas concentrations against W/F at A/F = 3 are presented in Figs. 2 and 3, respectively. Within the range of W/F where the autothermal reactions is sustained, the residual methane increases (i.e., methane conversion decreases) a little with increasing W/F. Carbon

Table 1b
Kinetic parameters

Reaction	K_{oj} (mol kgcat^{-1} s^{-1})	E_j (J mol^{-1})
1	9.287×10^2 bar$^{-1.5}$	30800
2	9.048×10^{11} bar$^{0.5}$	209500
3	5.43×10^5 bar^{-1}	70200
4	2.14×10^9 bar$^{0.5}$	211500

monoxide decreases and carbon dioxide increases gradually with increasing W/F due to the improved water-gas shift reaction. On the other hand, the content of water vapour increases dramatically in the wet product because the increase in the steam reforming reaction is not directly proportional to the increase in the W/F ratio. As a result, the wet hydrogen concentration decreases, although its concentration increases in the dry product. By contrast, the nitrogen concentration, decreases due to increase in the concentrations of water vapour and carbon dioxide in the product.

The methane conversion efficiency, which is defined as the difference in the moles of methane between the inlet and outlet of the reactor divided by the moles of methane supplied, at different A/F and W/F. The results show that methane conversion increases with increasing A/F from 2.5 to 3.5 and then approaches 100% in the full range of W/F under study. With A/F < 3.5, methane conversion deceases with increasing of W/F.
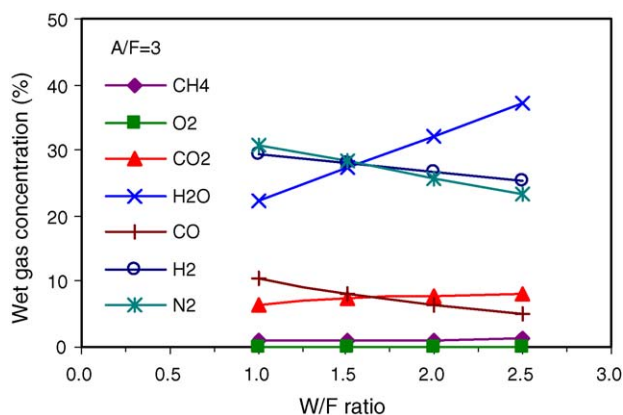
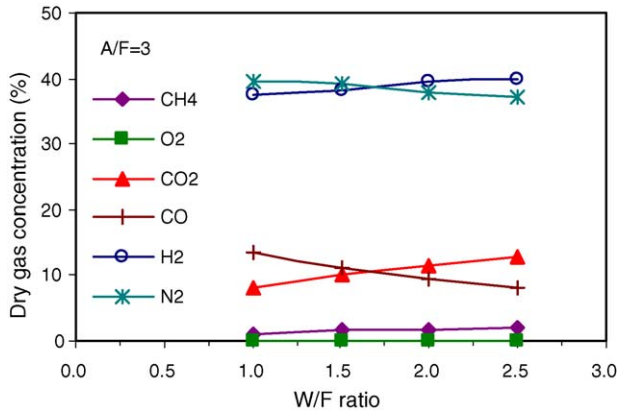Fig. 2. Wet product gas concentrations at different W/F ratios (A/F = 3, $V_{CH_4} = 120 l h^{-1}$).

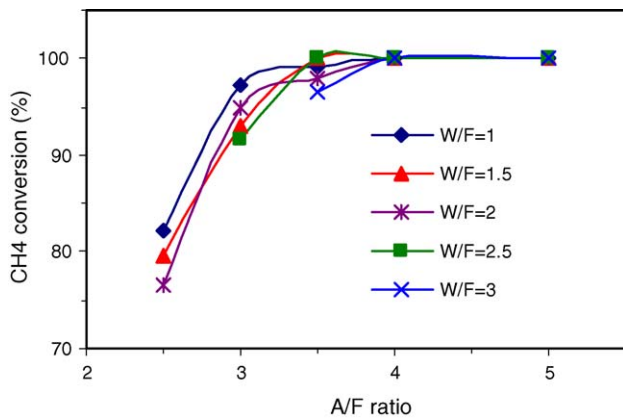Fig. 3. Dry product gas concentrations at different W/F ratios (A/F = 3, $V_{CH_4} = 120\,l\,h^{-1}$).

Fig. 6. Variation of hydrogen wet concentration vs. W/F ratio at different A/F ratios ($V_{CH_4} = 120\,l\,h^{-1}$).
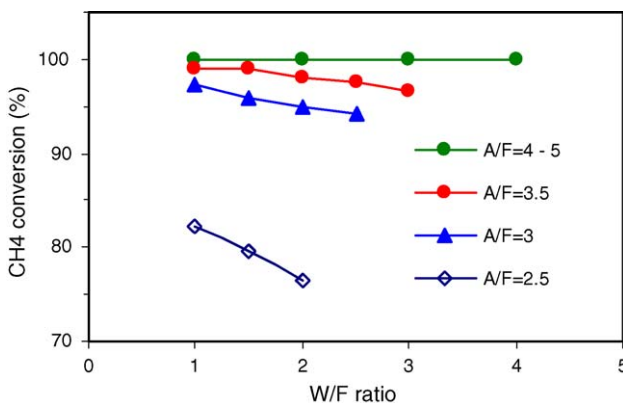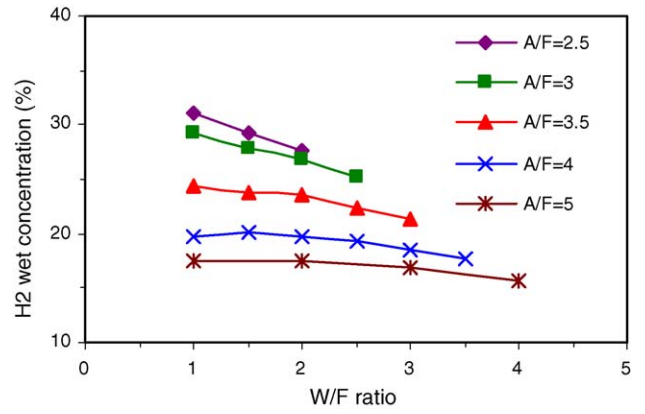

Fig. 4. Methane conversion vs. A/F ratio at different W/F ratios ($V_{CH_4} = 120\,l\,h^{-1}$).

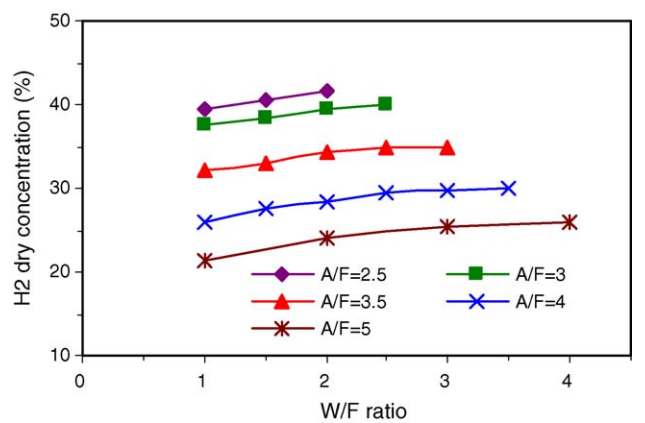Fig. 7. Variation of hydrogen dry concentration vs. W/F ratio at different A/F ratios ($V_{CH_4} = 120\,l\,h^{-1}$).

The variation of hydrogen concentration in wet and dry products is shown in Figs. 6 and 7, respectively, under different A/F and W/F. The concentration in both wet and dry products decreases with increasing of A/F due to the increase of nitrogen in the products. With a fixed A/F, the wet hydrogen concentration decreases with increasing W/F within the range studied, whereby the reactor can sustain autothermal reactions. This does not mean that the rate of hydrogen produced decreases with

increasing W/F because of the increased water vapour content in the products. When removing the water vapour from the products, the dry hydrogen concentration increases with increasing W/F, as indicated in Fig. 7.

The effect of W/F on the flow of hydrogen produced can be seen more clearly in Fig. 8, which shows that the moles of hydrogen produced per mole of methane fed into the reactor increases
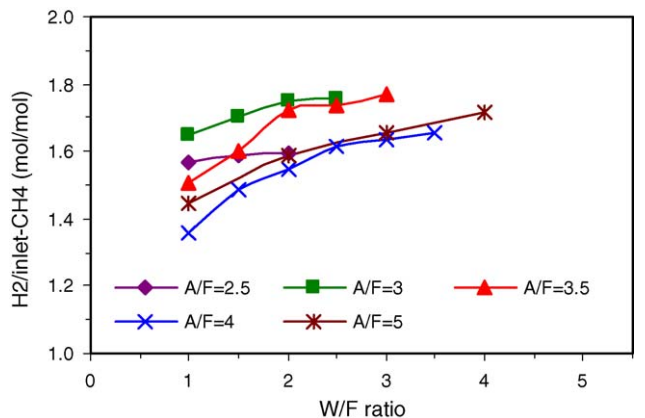

Fig. 5. Methane conversion vs. W/F ratio at different A/F ratios ($V_{CH_4} = 120\,l\,h^{-1}$).

Fig. 8. Mole of hydrogen produced per mole of methane fed into the reactor vs. W/F ratio at different A/F ratios ($V_{CH_4} = 120\,l\,h^{-1}$).
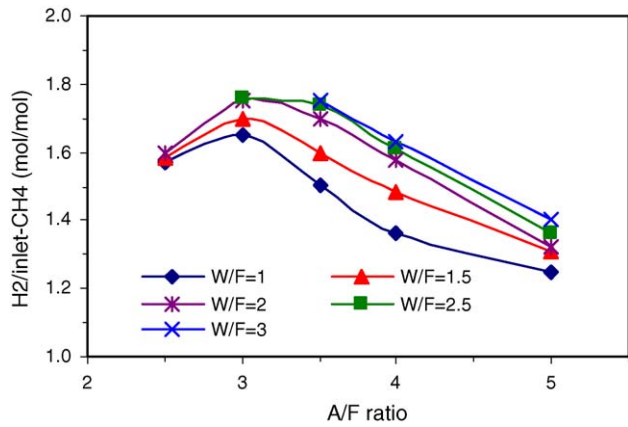
Fig. 9. Mole of hydrogen produced per mole of methane fed into the reactor vs. A/F ratio at different W/F ratios ($V_{CH_4} = 120 \, l \, h^{-1}$).
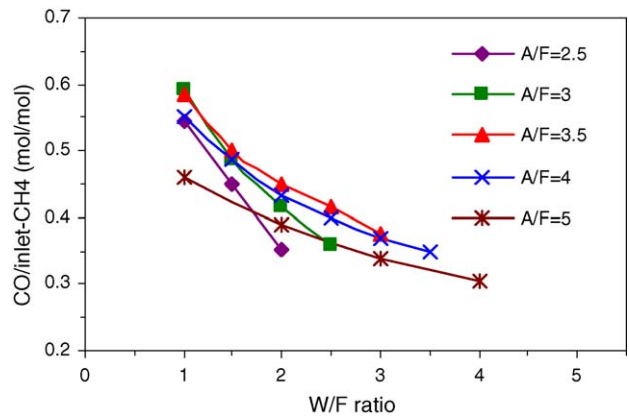

Fig. 12. Mole of carbon monoxide produced per mole of methane fed into the reactor vs. W/F ratio at different A/F ratios ($V_{CH_4} = 120 \, l \, h^{-1}$).
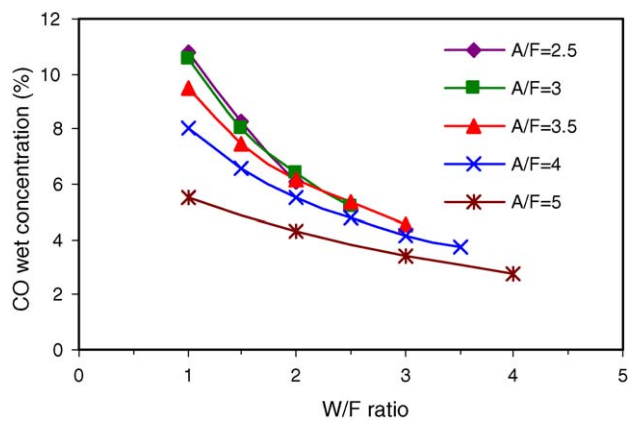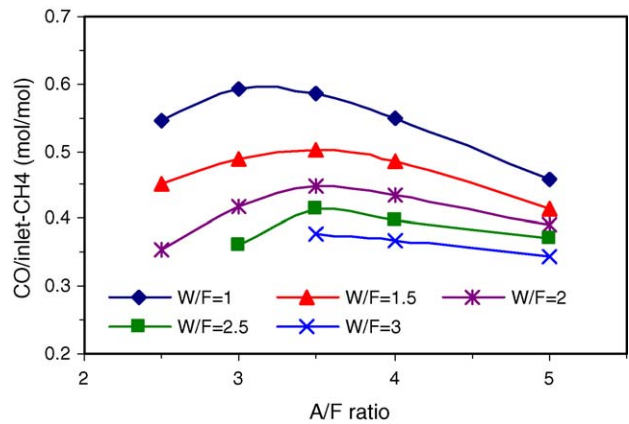

Fig. 10. Variation of carbon monoxide wet concentration vs. W/F ratio at different A/F ratios ($V_{CH_4} = 120 \, l \, h^{-1}$).

Fig. 13. Mole of carbon monoxide produced per mole of methane fed into the reactor vs. A/F ratio at different W/F ratios ($V_{CH_4} = 120 \, l \, h^{-1}$).

with increasing W/F. On lowering the A/F, the maximum W/F at which the reactor can sustain an autothermal reaction is lowered due to the reduced heat release to vaporize water and to compensate the endothermic steam reforming reaction.

The effect of A/F on the moles of H_2 produced, on the other hand, is different as can be seen in Fig. 9. The moles of H_2 produced reaches a peak for A/F ratios between 3 and 3.5 with a W/F ratio of 2–2.5. Under these mixture conditions, the maxi-

mum moles of hydrogen is about 1.8 moles per mole of methane supplied and the wet and dry hydrogen concentrations reach 28 and 40%, respectively.

The variation of CO concentrations and CO moles against A/F and W/F ratios is shown in Figs. 10–13. Both wet and dry CO concentrations and the moles of CO produced per mole of methane dramatically decrease with increasing W/F. This is
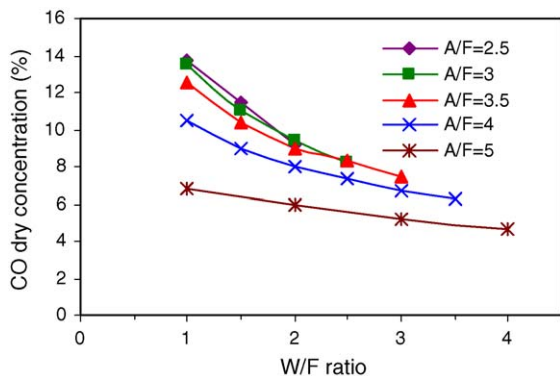

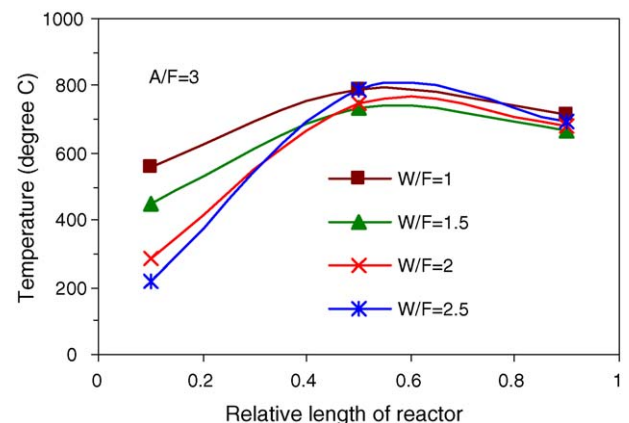Fig. 11. Variation of carbon monoxide dry concentration vs. W/F ratio at different A/F ratios ($V_{CH_4} = 120 \, l \, h^{-1}$).

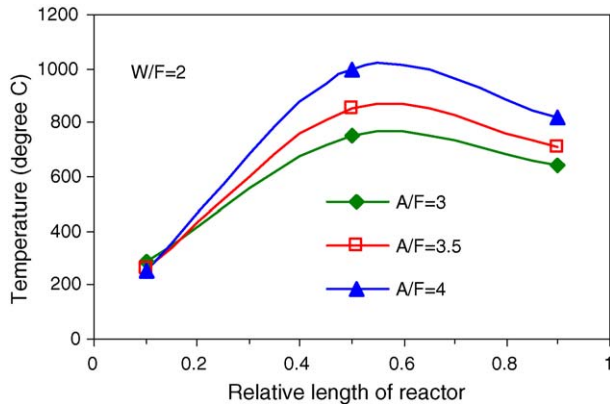Fig. 14. Catalyst temperature along reactor at different W/F ratios (A/F = 3, $V_{CH_4} = 120 \, l \, h^{-1}$).

Fig. 15. Catalyst temperature along reactor at different A/F ratios (W/F = 2, $V_{CH_4} = 120 \, l \, h^{-1}$).

Fig. 17. Methane conversion vs. methane flowrate (A/F = 3, W/F = 2).

because of increase in the water-gas shift reaction in the reactor. The effect of A/F on CO generation is similar to that on hydrogen generation. With an A/F of 3–3.5 and a W/F of 2–2.5, the wet CO concentration is as low as 5–7%, the dry CO concentration is 7–9% and the moles of CO is as low as 0.4–0.45 per mole of methane supplied.

The distribution of catalyst temperature in the reactor at different W/F and A/F ratios is shown in Figs. 14 and 15, respectively. In general, the catalyst temperature is lowest in the front part, highest in the middle part and lower in the rear part of the reactor. This can be explained as follows: the front part is cooled by the inlet mixture of low temperature, the middle part is heated by heat release from the total combustion of methane, while the endothermic steam reforming reaction is prominent, in the rear part the reactor. Increasing W/F leads to more cooling of the front part, which causes the temperature in this area to decrease. As a result, more of the total combustion reaction of methane shifts to the middle part and increases temperature there (Fig. 14). At a fixed W/F, an increase in A/F means an increase in the combustion rate and heat release and, hence, the reactor temperature increases (Fig. 15).

The effect of inlet methane flowrate on the reforming performance is presented in Figs. 16–18, which show gas concentrations in the wet product, methane conversion and moles of
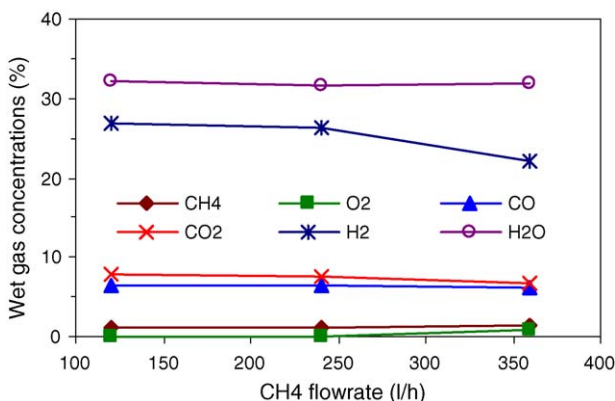
hydrogen produced per mole of methane under different flow rates of methane feed at A/F = 3 and W/F = 2. Increasing the rate of methane feed beyond $250 \, l \, h^{-1}$ will decrease methane conversion (Fig. 17). This leads to a decrease in H_2 concentration in the products and the moles of H_2 produced per mole of CH_4 feed (Fig. 18). The decrease in methane conversion with increasing feed flowrate is due mainly to the change of temperature profile in the reactor. With the flowrate of feed gas exceeding a certain value ($250 \, l \, h^{-1}$ in the present experiment), a higher flowrate will cause more cooling of the front part of the reactor and result in more inactive catalyst and, hence, a lower chemical reaction rate.

Based on the results presented and discussed above, it can be seen that the optimum operating conditions for the autothermal reactor to achieve high hydrogen yield, a high methane conversion and a high number of moles of hydrogen produced per mole of methane feed are an A/F of 3–3.5 and a W/F of 2–2.5 under a flowrate of methane of $120–250 \, l \, h^{-1}$. With these conditions, methane conversion can reach 95–99%; to the hydrogen concentration can reach 39–41% of dry products (28–30% wet products); the moles of hydrogen can reach 1.8 per mole of methane feed CO concentration can be as low as 7–9% dry (5–7% wet) and the number of CO moles can be as low as 0.4–0.5 per mole of methane feed. Under these feed conditions, the maximum catalyst temperature will not exceed 850 °C.
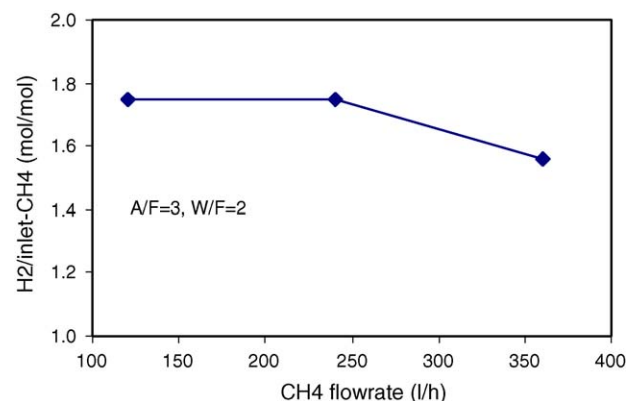

Fig. 16. Wet product gas concentrations at different methane flowrates (A/F = 3, W/F = 2).
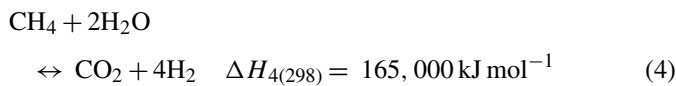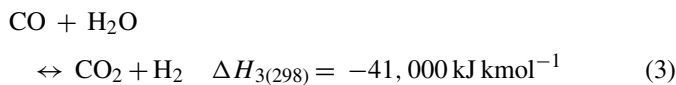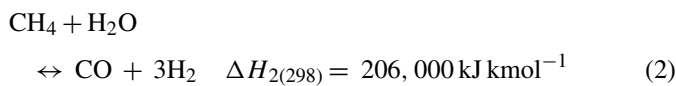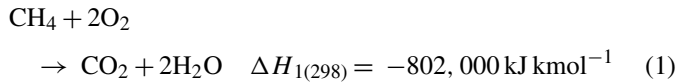

Fig. 18. Mole of hydrogen produced per mole of methane fed into the reactor vs. methane flowrate (A/F = 3, W/F = 2).

3. Mathematical model

3.1. Chemical reaction scheme

In addition to the experimental investigation, modelling work has been conducted to examine further the conversion behaviour of the ATR process inside the reactor. The model includes detailed reactions associated with partial oxidation and steam reforming. The detailed analysis of chemical reactions in these processes to determine the reaction scheme for ATR has been presented elsewhere [10,11]. The main reactions considered in the model are as follows:

$$CH_4 + 2O_2 \rightarrow CO_2 + 2H_2O \quad \Delta H_{1(298)} = -802,000 \, kJ \, kmol^{-1} \quad (1)$$

$$CH_4 + H_2O \leftrightarrow CO + 3H_2 \quad \Delta H_{2(298)} = 206,000 \, kJ \, kmol^{-1} \quad (2)$$

$$CO + H_2O \leftrightarrow CO_2 + H_2 \quad \Delta H_{3(298)} = -41,000 \, kJ \, kmol^{-1} \quad (3)$$

$$CH_4 + 2H_2O \leftrightarrow CO_2 + 4H_2 \quad \Delta H_{4(298)} = 165,000 \, kJ \, mol^{-1} \quad (4)$$

Thus, the model takes into account four reactions (1)–(4) and six gas species, i.e., methane, oxygen, carbon dioxide, water, carbon monoxide and hydrogen, nitrogen present in the inlet air is considered as a diluent, which affects only the gas properties.

Kinetic rate equations and kinetic data applied for sulfide nickel catalyst in this work are adopted from earlier studies with the same catalyst [10]. The rate equations and kinetic data for Eqs. (1)–(4) are as follows:

$$R_1 = \frac{k_1 p_{CH_4} p_{O_2}^{1/2}}{(1 + K_{CH_4}^C p_{CH_4} + K_{O_2}^C p_{O_2}^{1/2})^2} \quad (5)$$

$$R_2 = \frac{k_2}{p_{H_2}^{2.5}} \left(p_{CH_4} p_{H_2O} - \frac{p_{H_2}^3 p_{CO}}{K_{e2}} \right) \times \frac{1}{Q_r^2} \quad (6)$$

$$R_3 = \frac{k_3}{p_{H_2}} \left(p_{CO} p_{H_2O} - \frac{p_{H_2} p_{CO_2}}{K_{e3}} \right) \times \frac{1}{Q_r^2} \quad (7)$$

$$R_4 = \frac{k_4}{p_{H_2}^{3.5}} \left(p_{CH_4} p_{H_2O}^2 - \frac{p_{H_2}^4 p_{CO_2}}{K_{e4}} \right) \times \frac{1}{Q_r^2} \quad (8)$$

$$Q_r = 1 + K_{CO} p_{CO} + K_{H_2} p_{H_2} + K_{CH_4} p_{CH_4} + \frac{K_{H_2O} p_{H_2O}}{p_{H_2}}$$

where R_j (kmol kgcat^{-1} h^{-1}) is the rate of reaction j ($j = 1$–4); p_{CH_4}, p_{O_2}, etc. are, respectively, the partial pressures of gas species CH_4, O_2, etc.; $k_j = k_{oj} \times e^{-E_j/RT}$ is the kinetic rate constant of reactions j ($j = 1$–4) and is determined from Ref. [10]. The kinetic data are shown in Tables 1a and b, where k_{oj} is a constant, E_j (kJ kmol^{-1}) the activation energy; R (kJ kmol^{-1} K^{-1}) the universal gas constant; T (K) the gas temperature in the reaction zone; K_{ej} the equilibrium constant of

Table 2
Equilibrium constants

Reaction	Equilibrium constant K_{ej}
2	$5.75 \times 10^{12} \times e^{-95411/(RT)}$ (bar^2)
3	$1.26 \times 10^{-2} \times e^{38568/(RT)}$
4	$7.24 \times 10^{10} \times e^{-179960/(RT)}$ (bar^2)

Table 3
Adsorption constants

Species	K_{oi} (bar^{-1})	ΔH_i (J mol)
CH$_4$ (Combustion)	2.02×10^{-3}	-36330
O$_2$ (Combustion)	7.4×10^{-5} bar$^{0.5}$	-57970
CH$_4$	1.995×10^{-3}	-36650
CO	8.11×10^{-5}	-70230
H$_2$	7.05×10^{-9}	-82550
H$_2$O	1.68×10^4 bar	85770

reaction j ($j = 2$–4) Table 2; $K_i^C = K_{oi}^C \times e^{-\Delta H_i^C/RT}$ the adsorption constant of species i ($i = CH_4$, O_2) in oxidation reaction (1); $K_i = K_{oi} \times e^{-\Delta H_i/RT}$ the adsorption constant of species i ($i = CO$, H_2, CH_4, H_2O) in reforming reactions (2)–(4), which can be found in Table 3.

The rate of consumption or formation of an individual gas species based on reactions (1)–(4) is determined by summing up the reaction rates of that species in all four reactions, i.e.,

$$r_{CH_4} = -R_1 - R_2 - R_4 \quad (9)$$

$$r_{O_2} = -2R_1 \quad (10)$$

$$r_{CO_2} = R_1 + R_3 + R_4 \quad (11)$$

$$r_{H_2O} = 2R_1 - R_2 - R_3 - 2R_4 \quad (12)$$

$$r_{CO} = R_2 - R_3 \quad (13)$$

$$r_{H_2} = 3R_2 + R_3 + 4R_4 \quad (14)$$

where r_i is the conversion rate of gas species i ($i = CH_4$, O_2, etc.).

3.2. Model development

The schematic layout of the reactor is shown in Fig. 19. The reactor is of a cylindrical shape (30 mm in diameter and 200 mm in length) and is filled with a spherical sulfide Ni catalyst with a size of 1.75 mm and 9.8% active metal. Radiation in a catalyst bed can be significant only at temperatures above 1000 °C [17]. The maximum catalyst temperature in this study is less than this

Fig. 19. Schematic layout of 2-D reactor.

limit, and thus radiative heat transfer can be omitted. Moreover, because the gas flowrate is relatively low and the void fraction of the bed is high (0.35), the pressure drop is assumed to be negligible. To simplify the model, it may be assumed that the gas flow in the reactor is uniform, and thus a 1-D model can be used for the reactor. The radial dispersion of the gas flow due to a catalyst particle size of 1.75 mm and the radial heat transfer due to heat loss through the wall of the reactor may have some effects on the overall reforming performance. To take these effects into account, a 2-D reactor model is more appropriate to describe the reforming behaviour under the mentioned conditions [11,18]. Hence, a 2-D model is developed in this study. Since the dispersion coefficient in the axial direction is much smaller than the effect of gas velocity, it can be ignored without significant influence on the calculation results. In addition, the heat conductivity of the gas is much smaller than that of the catalyst bed, and therefore can be omitted. In the gas phase, changes in the gas properties and concentrations with time are normally much smaller than those with space, especially when the operation is in a quasi-steady state; hence they can be ignored within a small step time.

With the assumptions mentioned above, the basic governing equations of the model based on the mass and energy balance for the gas phase and solid phase of the reactor are as follows:

$$u \frac{\partial C_i}{\partial z} = D_{dpi} \left(\frac{\partial^2 C_i}{\partial r^2} + \frac{1}{r} \frac{\partial C_i}{\partial r} \right) + \rho_{cat} r_i \tag{15a}$$

$$\varepsilon \rho_g c_{pg} \frac{\partial T_g}{\partial t} = -u \rho_g c_{pg} \frac{\partial T_g}{\partial z} + S_h h (T - T_g) \tag{16}$$

$$\rho_b c_{pb} \frac{\partial T}{\partial t} = K \left(\frac{\partial^2 T}{\partial r^2} + \frac{1}{r} \frac{\partial T}{\partial r} + \frac{\partial^2 T}{\partial z^2} \right)$$

$$+ S_h h (T_g - T) + \rho_{cat} \sum_{j=1}^{4} (-\Delta H_j) R_j \tag{17a}$$

where i denotes the gas species; j denotes reaction index; ρ_g, ρ_{cat}, ρ_b (kg m^{-3}) the densities of gas, catalyst and bulk catalyst bed, respectively; c_{pg} and c_{pb} (J kg^{-1} K^{-1}) the specific heats of the gas and the catalyst bed, respectively; ε the void fraction of the catalyst bed; h_{Di} (m s^{-1}) the mass transfer coefficient of the gas component i; h (W m^{-3} K) the heat transfer coefficient; T and T_g (K) the temperature of solid phase and gas phase, respectively; C_i (mol m^{-3}) the concentration of gas species i; r and z (m) are cylindrical coordinates; S_h (m^{-2} m^{-3}) the heat transfer area per volume of the catalyst bed; ΔH_j (J mol^{-1}) the heat of reaction j; K (W m^{-1} K^{-1}) the heat conduction coefficient of the catalyst bed; D_{dpi} the dispersion coefficient of gas component i; u (m s^{-1}) is the superficial gas velocity equal to the ratio of the volume flow rate to the cross-section area of the reactor.

The dispersion coefficient of gas in a catalyst bed is dependent on molecular gas diffusion, bulk gas velocity and pellet diameter and can be expressed as [19]:

$$D_{dpi} = \varepsilon \left(\frac{D_i}{\tau_{bed}} + 0.5 d_p u \right)$$

where d_p is pellet diameter; D_i the gas diffusivity of species i to the mixture of the other gas in the reactor; τ_{bed} is tortuosity of the bed and is correlated to the void fraction of the catalyst bed ε as follows [20]:

$$\tau_{bed} = \frac{1}{\sqrt{\varepsilon}}$$

Based on the phenomena of the gas flow and operating conditions of the reactor, the initial and boundary conditions are set as follows:

$$\text{initial condition } t = 0: \quad T = T_o; \tag{18}$$

$$\text{at the reactor inlet face } z = 0: \quad T_g = T_g^{in}; C_i = C_i^{in} \tag{19}$$

$$\text{at the reactor outlet face } z = L: \quad \frac{\partial C_i}{\partial z} = 0; \quad \frac{\partial T_g}{\partial z} = 0 \tag{20}$$

$$\text{at the reactor centre } r = 0: \quad \frac{\partial C_i}{\partial r} = 0; \quad \frac{\partial T_g}{\partial r} = 0 \tag{21}$$

With these conditions, Eqs. (15a) and (17a) can be replaced by Eqs. (15b) and (17b), respectively, i.e.,

$$u \frac{\partial C_i}{\partial z} = 2 D_{dpi} \frac{\partial^2 C_i}{\partial r^2} + \rho_{cat} r_i \tag{15b}$$

$$\rho_b c_{pb} \frac{\partial T}{\partial t} = K \left(2 \frac{\partial^2 T}{\partial r^2} + \frac{\partial^2 T}{\partial z^2} \right)$$

$$+ S_h h (T_g - T) + \rho_{cat} \sum_{j=1}^{4} (-\Delta H_j) R_j \tag{17b}$$

At the interfacial surface of the inner reactor wall and the catalyst bed $r = R$:

$$\frac{\partial C_i}{\partial r} = 0; \quad K \frac{\partial T}{\partial r} = \alpha (T - T_a) \tag{22}$$

where T_a is the ambient temperature; α the overall heat transfer coefficient through the reactor wall; K (W m^{-1} K^{-1}) is the heat conduction coefficient of the catalyst bed.

The heat transfer coefficient between the catalyst and the gas, h (W m^{-2} K^{-1}), is determined using the Colburn factor [21]. The overall heat transfer coefficient through the reactor wall, α, is determined from:

$$\frac{1}{\alpha} = \frac{1}{h_i} + \frac{b}{\lambda} + \frac{1}{h_o} \tag{23}$$

where b is thickness of the reactor wall including the insulation layer (m); h_i and h_o are the heat transfer coefficient on the inside and outside of the reactor wall (W m^{-2} K^{-1}), respectively, while λ the heat conduction coefficient of the reactor wall (W m^{-1} K^{-1}), which can be taken from Ref. [22]; h_i is given by Cussler [23] and h_o for free convection is taken from Ref. [11,24].

The set of three governing Eqs. (15)–(17) with Eqs. (18)–(22) for the initial and boundary conditions, combined with the heat and mass transfer coefficients is then solved for the temperature and gas concentration along and across the reactor using a finite
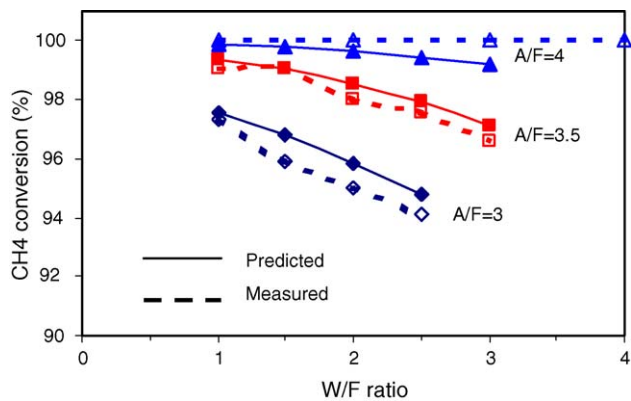
Fig. 20. Comparison between predicted and measured methane conversions at different W/F and A/F ratios ($V_{CH_4} = 120\,1\,h^{-1}$).

difference method. The overall temperature and compositions of the products are obtained from the predicted values at different space elements at the rear face of the reactor.

3.3. Modelling results

The program code is run under initial catalyst temperature $T_0 = 673\,K$ (400 °C), at which the reactor can light-off and sustain autothermal reactions [11]. The inlet mixture compositions and flowrate are set to the same values as that of the experiment carried out previously. When the reactor is at a fully steady-state (all output parameters are stable), the gas parameter inside the reactor and the product compositions are extracted. Some typical predicted data under a fuel flowrate of $V_{CH_4} = 120\,1\,h^{-1}$ are presented in Figs. 20–25.

The predicted and measured conversion of methane under different W/F and A/F are compared in Fig. 20. There is quite good agreement between the two sets of data. The agreement between modelling and experimental results is also seen in Fig. 21, which shows the dry gas product concentrations at A/F = 3 and different W/F. With this successful validation, the simulation program code can be used to study the conversion behaviour inside the reactor.
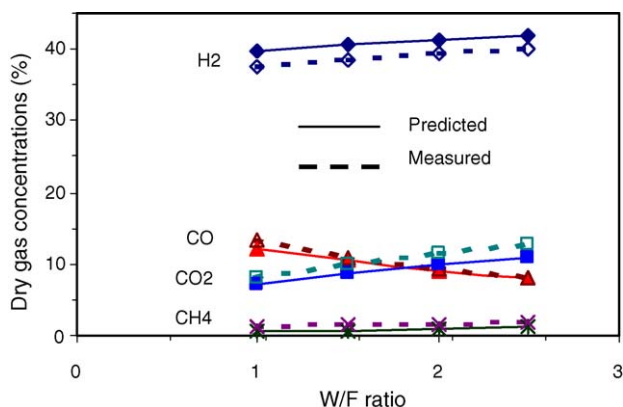

Fig. 21. Comparison between predicted and measured gas concentrations at different W/F ratios (A/F = 3, $V_{CH_4} = 120\,1\,h^{-1}$).
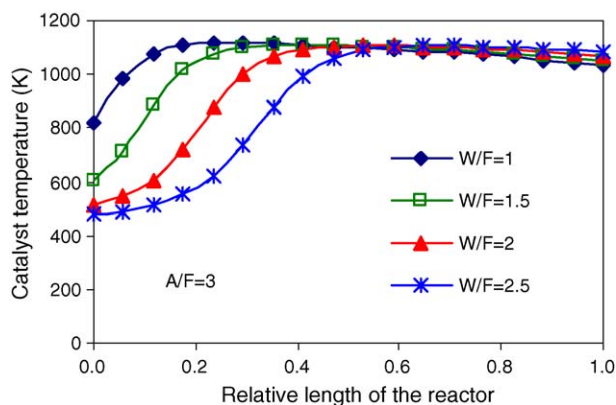

Fig. 22. Predicted catalyst temperature along the reactor at different W/F ratios (A/F = 3, $V_{CH_4} = 120\,1\,h^{-1}$).
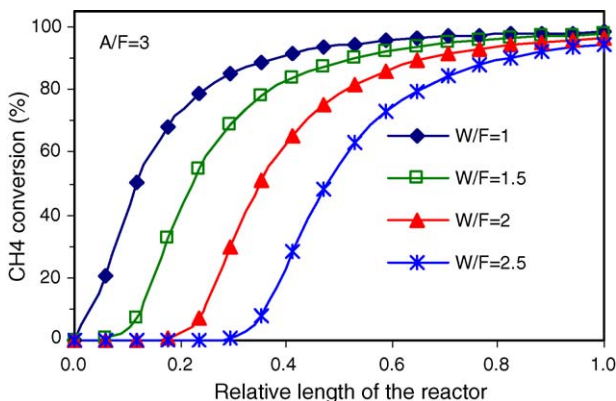

Fig. 23. Predicted methane conversion inside the reactor at different W/F ratios (A/F = 3, $V_{CH_4} = 120\,1\,h^{-1}$).

The catalyst temperature along the reactor at A/F = 3 and different W/F is given in Fig. 2. Increasing water content at the inlet leads to a change in the temperature profile of the catalyst bed. The front part of the reactor is cooled down with increasing W/F. This then causes the methane conversion to decrease sharply in the front part of the reactor, as seen in Fig. 23, and hence results in a decrease in the overall conversion.

The formation of hydrogen and carbon monoxide in the reactor is shown in Figs. 24 and 25, respectively, the decrease in
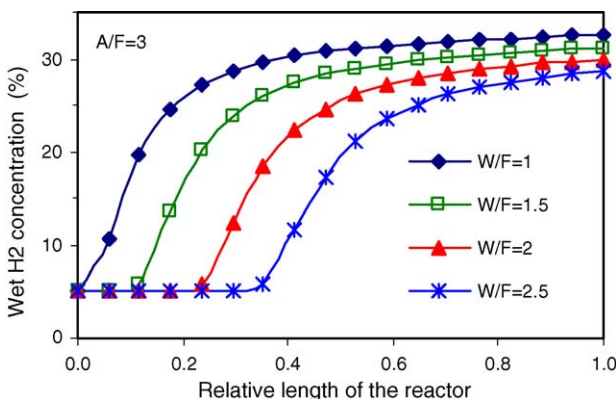

Fig. 24. Predicted wet hydrogen concentration inside the reactor at different W/F ratios (A/F = 3, $V_{CH_4} = 120\,1\,h^{-1}$).
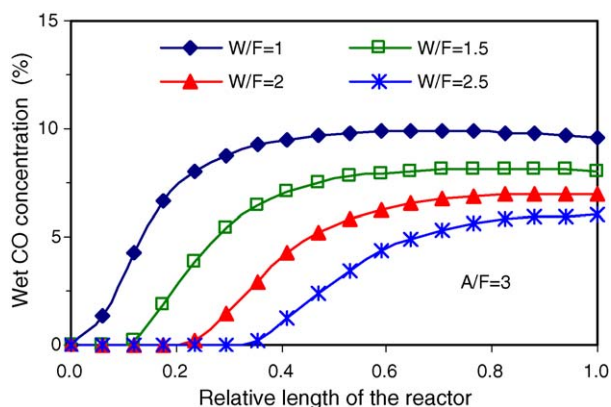
Fig. 25. Predicted wet carbon monoxide concentration inside the reactor at different W/F ratios (A/F = 3, $V_{CH_4} = 120\,l\,h^{-1}$).

hydrogen formation with increasing W/F is a consequence of the decrease in methane conversion presented in Fig. 23. The decrease of carbon monoxide, on the other hand, is due to the improved water-gas shift reaction at lower temperature and high water content.

The simulation code allows determination of all the gas parameters and the catalyst temperature at any position inside the reactor and, hence, it can be used to study the factors that influence the reforming performance and for optimum reactor design.

4. Conclusions

Autothermal reforming of methane over a sulfide nickel catalyst is investigated experimentally and theoretically. The experiments are carried out under thermally neutral conditions in a cylindrical reactor of 30 mm in diameter and 200 mm in length. The results show that the conversion behaviour of the reactor strongly depends on A/F, W/F and the inlet mixture flowrate. The optimum condition of autothermal methane reforming is found at a molar A/F of 3–3.5, a molar W/F of 2–2.5 and a fuel flowrate below $250\,l\,h^{-1}$. Under these conditions, methane conversion is 95–99%; the hydrogen yield the 39–41% on a dry basis, and 1 mole of methane can produce 1.8 moles of hydrogen. The carbon monoxide concentration is as low as 7–9% on a dry basis (5–7% on a wet basis), or 0.4–0.5 mole per mole of methane feed.

A two-dimensional heterogeneous reactor model has been successfully developed and validated. The study considers four main simultaneous chemical kinetic reactions that involve six species with detailed kinetic conversion and heat and mass transfer phenomena in the reactor. The model is useful for analysis of the factors that influence the reforming performance and for optimum reactor design.

References

[1] S. Ahmed, M. Krumpelt, Int. J. Hydrogen Energy 26 (2001) 291–301.
[2] S.H. Chan, O.L. Ding, D.L. Hoang, Int. J. Green Energy 1 (2004) 265–278.
[3] J. Xu, G.F. Froment, AIChE J. 35 (1989) 88–96.
[4] G. Barbieri, F.P. Di Maio, Ind. Eng. Chem. Res. 36 (1997) 2121–2127.
[5] K. Hou, R. Hughes, Chem. Eng. J. 82 (2001) 311–328.
[6] H.M. Kvamsdal, H.F. Svendsen, T. Hertzberg, O. Olsvik, Chem. Eng. Sci. 54 (1999) 2697–2706.
[7] A.M. De Goote, G.F. Froment, Appl. Catal. A 138 (1996) 245–264.
[8] A. Basile, L. Paturzo, F. Lagana, Catal. Today 67 (2001) 65–75.
[9] T. Ostrowski, A. Giroir-Fendler, C. Mirodatos, L. Mleczko, Catal. Today 40 (1998) 181–190.
[10] D.L. Hoang, S.H. Chan, O.L. Ding, Chem. Eng. Res. Des. 83 (2005) 177–186.
[11] D.L. Hoang, S.H. Chan, Appl. Catal. A 268 (2004) 207–216.
[12] T. Takeguchi, S.-N. Furukawa, M. Inoue, K. Eguchi, Appl. Catal. A: Gen. 240 (2003) 223–233.
[13] J.A.C. Dias, J.M. Assaf, J. Power Sources 130 (2004) 106–110.
[14] M.M.V.M. Souza, M. Schmal, Appl. Catal. A 281 (2005) 19–24.
[15] K. Nagaoka, A. Jentys, J.A. Lercher, J. Catal. 229 (2005) 185–196.
[16] S.H.D. Lee, D.V. Applegatea, S. Ahmeda, S.G. Calderoneb, T.L. Harvey, Int. J. Hydrogen Energy 30 (2005) 829–842.
[17] D. Wolf, M. Hohenberger, M. Baerns, Ind. Eng. Chem. Res. 36 (1997) 3345–3353.
[18] S. Grevskott, T. Rusten, M. Hillestad, E. Edwin, O. Olsvik, Chem. Eng. Sci. 56 (2001) 597–603.
[19] N. Wakao, S. Kaguei, T. Funazkri, Chem. Eng. Sci. 34 (1979) 325–336.
[20] M. Puncochar, J. Drahos, Chem. Eng. Sci. 48 (1993) 2173–2175.
[21] R.B. Bird, W.E. Stwewart, E.N. Lightfoot, Transport Phenomena, John Wiley & Sons, New York, USA, 1960.
[22] A.J. Chapman, Heat Transfer, Macmillan Publishing Co., New York, USA, 1984.
[23] E.L. Cussler, Diffusion, Mass Transfer in Fluid Systems, Cambridge University Press, Cambridge, UK, 1984.
[24] S.W. Churchill, H.H.S. Chu, Int. J. Heat Mass Transfer 18 (1975) 1049–1053.